HIGH FREQUENCY INSTABILITIES IN ROCKET THRUST CHAMBERS
AN ENGINEERING APPROACH

*F. A. Fassl**

Astrium GmbH, Business Division Launcher Propulsion

81663 München, Germany

Abstract

The prediction and prevention of high frequency instabilities in rocket engines remains a challenging task not only for science to understand the ruling processes and to measure, simulate and model them, but also for industry to find pragmatic ways to combine existing knowledge and experimental experience from laboratory or industrial full scale tests and to apply them systematically already in the early stages of rocket engine development programs. The French- German REST program constitutes a scientific platform aiming at combining both scientific investigation and industrial viewpoint.

The concept of Astrium's stability analysis tool STABAN was elaborated in REST and systematically developed and adjusted. It constitutes an engineering approach in the frequency domain enabling a quick applicability to any engine hardware. In future REST phases, the main focus will be the validation of STABAN to scientific and industrial test data and to classify thrust chambers into instability risk families.

Nomenclature (all quantities in SI units if not dimensionless)

a	sonic velocity
A	sectional area
A_{nm}	factor for the additional driving terms
c*	characteristic velocity
C	capacitance
d	droplet diameter
G	combustion gain
l^*	characteristic length
m	mass
Ma	Mach number
n	interaction index for combustion gain
P	pressure
r	injection mixture ratio
R	resistance
$s=\lambda+i\cdot\omega$	Laplace variable
T	period time
x	combustion chamber axis
Y	admittance
λ	system eigenvalue
η	efficiency
κ	isentropic exponent
ρ	density
τ	time lag
ω	circular system eigenfrequency

Subscripts:

abs	absorber
c	combustion chamber or hot gas
DD	droplet drag
drop	propellant droplet
fu	fuel
inj	at injection
ms	mass storage
ni	nozzle inlet
ox	oxidizer
Pc	chamber pressure- related
rel	normalized
s	sensitive
t	total
vc	gas velocity- realted

1 Introduction

An extensive experimental data base exists at Astrium from the past decades of thrust chamber testing for ARIANE 5. This data base encompasses a large variety of thrust chambers extending from subscale testing on quasi scientific level to full scale development, acceptance and qualification tests, and that for hypergolic, green and cryogenic propellants with different injection system designs and operation conditions. This enables a systematic exploitation for trend analyses and to extract a family behavior for an early definition of the development direction for future thrust chamber designs.

* Company Expert in *Stage/ Propulsion Functional Engineering & Performance*

The French- German REST group, dedicated to an enlarged understanding of processes leading to HF instability in rocket engines, follows the derivation of physical correlations for significant stability parameters and processes and supports the development, testing and validation of predictive tools for industrial use. Experimental data are created in laboratory scale completing the industrial test data bases and the engineering knowledge.

In the scope of REST, the STABAN code is developed at Astrium for systematic analyses of experimental data for a stability- related data base as well as for predictions for future engine concepts or for extrapolations from subscale to full scale hardware. The modeling concept and some practical examples of application are presented.

2 Modeling Approach

The following figure depicts the main players in stability physics which are considered in STABAN. On the left side the hardware of one of Astrium's thrust chambers is shown.

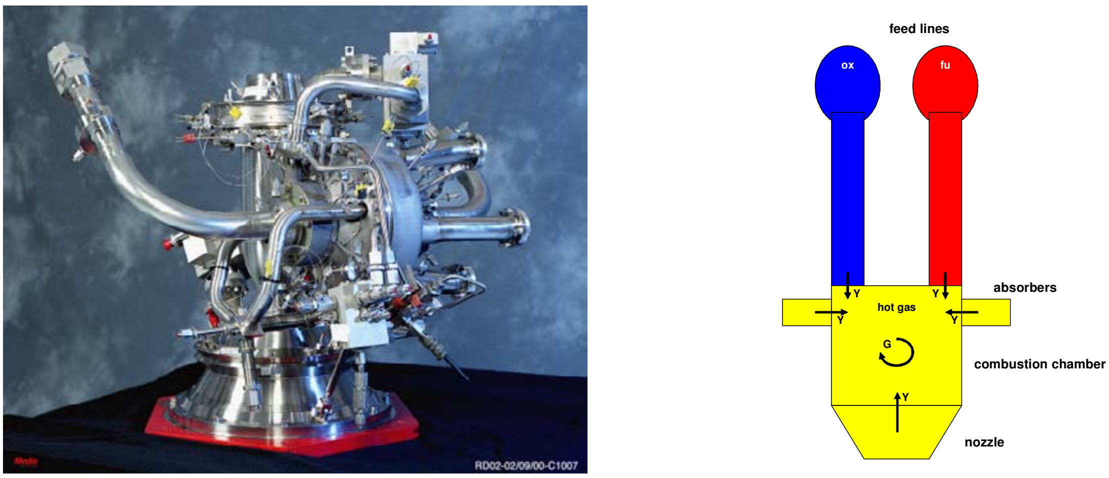

Fig. 2/1 Coupled System Stability Model

All system parts connected to the combustion chamber are represented by their admittances Y. The dynamic impact of the propellants at the time of injection is considered as well as the one of the convergent part of the exhaust nozzle. Admittance is also provided by intentionally incorporated damping devices. An intrinsic admittance is the droplet drags from the evaporating propellants. Against these admittances acts the combustion gain G as the main driving process for instability initiation. It describes the dynamic coupling of the combustion chamber pressure with the provision of ignitable propellant gas. All other intrinsic combustion chamber physics is combined in the additional driving terms D for oxidizer and fuel (see equation (2)).

System Model

Equation (1) describes a general propulsion system which can be tailored to the actual conditions and reduced to the effective system parts by appropriately modifying the sub-models and the model parameters.

$$G_{rel} + D_{ox.rel} + D_{fu.rel} = Y_{rel} \tag{1}$$

$$D_{ox.rel} = A_{nm} \cdot \frac{\bar{r}}{(\bar{r}+1)} \cdot \frac{\bar{P}_c}{2 \cdot \Delta \bar{P}_{inj.ox}} \cdot (1+k_{ox}) \cdot (1+s\cdot\Theta_{ox}) \cdot e^{-\bar{\tau}_{t.ox}\cdot s} \cdot Y_{inj.ox.rel} \tag{2}$$

$$D_{fu.rel} = A_{nm} \cdot \frac{1}{(\bar{r}+1)} \cdot \frac{\bar{P}_c}{2 \cdot \Delta \bar{P}_{inj.fu}} \cdot (1+k_{fu}) \cdot (1+s\cdot\Theta_{fu}) \cdot e^{-\bar{\tau}_{t.fu}\cdot s} \cdot Y_{inj.fu.rel}$$

$$Y_{rel} = Y_{ms.rel} + Y_{Pc.rel} + Y_{vc.rel} + Y_{DD.rel} + Y_{abs.rel} \tag{3}$$

The intrinsic combustion chamber physics and the effects from its interfaces to the surrounding system are arranged such that all processes having the potential to drive instability are combined on the left side and all processes supposed to damp are on the right side of equation (1). They are the combustion gain G_{rel}, the additional driving terms D_{rel} for oxidizer and fuel, respectively, and the damping admittances Y_{rel}. Tab. 2/1 summarizes all terms in the equations (1), (2) and (3), which base on fundamental considerations in [1].

Equation (1) is generally valid, still, low frequency (LF) and high frequency (HF) oscillations must be differently treated to account for the different physical impacts of the processes. Tab. 2/1 distinguishes between the linear and the non- linear oscillation case, the LF and the HF ranges and the oscillation modes. Thereby, TxRx means pure transversal modes (tangential and/or radial) and TxRxLx stands for longitudinal or combined modes (longitudinal mode with/ without transversal modes).

In line 1.1 of tab. 2/1 the pressure- dependent (linear) combustion gain is given which is only needed for HF investigations. This derives from the fact that the combustion chamber is treated as a black box for LF analyses without the need for resolving intrinsic physics. The linear combustion gain is extended by a non-linear term to consider the effect of flow velocity variation. Since flow velocity is a three- dimensional quantity and STABAN is not capable of spatially resolving the combustion chamber, the parameter $G_{vc.rel}$ must be empirically determined from test data, typically from time intervals with limit cycle oscillations of the combustion chamber pressure. The amplification factor F(u) in line 10.1 is only calculated when a critical value of the gas velocity amplitude is surpassed, otherwise it is zero. In fig. 2/2 a similar case is presented for a critical pressure amplitude level only beyond which instability is initiated.

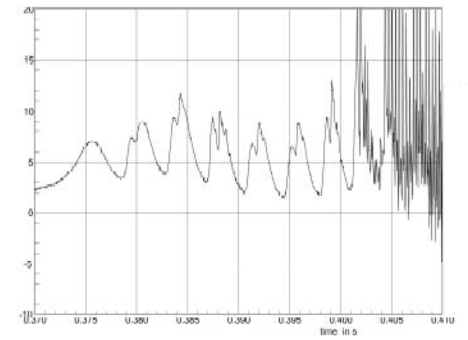

Fig. 2/2 HF Instability Initiation by LF Oscillation

The lines 1.1 and 1.2 only hold, if a condensed combustion is presumed in a flame front below the face plate. If the combustion is distributed along the combustion chamber axis, line 1.3 becomes relevant to get the integral value with the longitudinal chamber mode shape of a closed- closed oscillator. In STABAN a distributed combustion is not considered yet. This is an option for a future model extension. Anyhow, the condensed combustion constitutes the worst case for instability initiation.

In equation (2) the parameters k_{ox} and k_{fu} appear. They correspond to the steady- state gas mass flow from equation (8) and are, therefore, only applicable to the LF oscillation case for which the combustion chamber is considered as a black box. Equation (8) also delivers $Y_{Pc.rel}$ (line 5) and $Y_{vc.rel}$ (line 6) in the LF range.

Whereas the factors $(1+k_{ox})$ and $(1+k_{fu})$ as well as the admittances $Y_{Pc.rel}$ and $Y_{vc.rel}$ consider the impact of the hot gas flow in the combustion chamber and the convergent nozzle part, the factors $(1+s\cdot\Theta_{ox})$ and $(1+s\cdot\Theta_{fu})$ in equation (2) symbolize the impact of pulsing mass accumulation in the combustion chamber originating from the following physical processes:

- varying total combustion time lags making quicker droplets surpass slower ones (Klystron effect)

- varying sensitive time lag leading to a pulsing combustion
- pulsing coolant film consumption (only in case the combustion chamber wall is film cooled)

Case		Linear Oscillations			Non- Linear Oscillations	
Range		LF	HF			
Mode			TxRx	TxRxLx	TxRx	TxRxLx
1.1	$G_{Pc.rel}$	0	$A_c \cdot n \cdot \left(1 - e^{-\bar{\tau}_s \cdot s}\right)$			
1.2	G_{rel}	$G_{Pc.rel}$			$G_{Pc.rel} \cdot \left(1 + G_{vc.rel} \cdot F(u)\right)$	
1.3		$\int_0^1 G_{rel}(\hat{x}) \cdot d\hat{x}$		$\int_0^1 G_{rel}(\hat{x}) \cdot \cos\left(\omega \cdot \frac{T}{2} \cdot \hat{x}\right) \cdot d\hat{x}$	$\int_0^1 G_{rel}(\hat{x}) \cdot d\hat{x}$	$\int_0^1 G_{rel}(\hat{x}) \cdot \cos\left(\omega \cdot \frac{T}{2} \cdot \hat{x}\right) \cdot d\hat{x}$
2.1	k_{ox}	$(\bar{r}+1) \cdot \left(\frac{1}{\bar{c}^*} \cdot \frac{\partial c^*}{\partial r} + \frac{1}{\bar{\eta}_{c^*}} \cdot \frac{\partial \eta_{c^*}}{\partial r}\right)$	0			
2.2	k_{fu}	$-\bar{r} \cdot k_{ox}$	0			
3.1	Θ_{ox}	$\frac{\bar{\tau}_{t.ox}}{k_{ox}+1}$	$f_{Kly.ox} \cdot \bar{\tau}_{t.ox} - n_{32} \cdot \bar{\tau}_s \cdot \frac{\bar{r}+1}{\bar{r}}$			
3.2	Θ_{fu}	$\frac{\bar{\tau}_{t.fu}}{k_{fu}+1}$	$f_{Kly.fu} \cdot \bar{\tau}_{t.fu} \cdot \left(f_{fu} \cdot \frac{\bar{\rho}_c}{\bar{\rho}_{i.fu}} + 1\right) + n_{32} \cdot \bar{\tau}_s \cdot (\bar{r}+1)$			
4	$Y_{ms.rel}$	$s \cdot \Theta_c$				
5	$Y_{Pc.rel}$	1	$\frac{1}{\kappa}$	$\frac{1}{\kappa} \cdot \int_0^1 \hat{v}_{c.rel}(\hat{x}) \cdot \sin\left(\omega \cdot \frac{T}{2} \cdot \hat{x}\right) \cdot d\hat{x}$	$\frac{1}{\kappa}$	$\frac{1}{\kappa} \cdot \int_0^1 \hat{v}_{c.rel}(\hat{x}) \cdot \sin\left(\omega \cdot \frac{T}{2} \cdot \hat{x}\right) \cdot d\hat{x}$
6	$Y_{vc.rel}$	$-\frac{\bar{P}_c}{\bar{c}^*} \cdot \frac{\partial c^*}{\partial P_c} - \frac{\bar{P}_c}{\bar{\eta}_{c^*}} \cdot \frac{\partial \eta_{c^*}}{\partial P_c}$	$\frac{\alpha_{irr}}{\kappa \cdot Ma_{ni}}$			
7	$Y_{DD.rel}$	$\frac{1}{\bar{r}+1} \cdot \left(\bar{r} \cdot \frac{df_{DD.ox}}{dP_c} + \frac{df_{DD.fu}}{dP_c}\right)$				
8.1	$Y_{inj.ox.rel}$	$\frac{2 \cdot \Delta\bar{P}_{inj.ox}}{\bar{\dot{m}}_c} \cdot \frac{\bar{r}+1}{\bar{r}} \cdot Y_{inj.ox}$				
8.2	$Y_{inj.fu.rel}$	$\frac{2 \cdot \Delta\bar{P}_{inj.fu}}{\bar{\dot{m}}_c} \cdot (\bar{r}+1) \cdot Y_{inj.fu}$				
9	$Y_{abs.rel}$	$\eta_{abs} \cdot \frac{\bar{P}_c}{\bar{\dot{m}}_c} \cdot Y_{abs}$				
10.1	$F(u)$	0			$\frac{P_c'}{\bar{\rho}_c \cdot \bar{a}_c^2 \cdot Ma_c}$	
10.2	$K(\hat{x})$	0	$\frac{\hat{k}(\hat{x})}{\kappa} \cdot \frac{1-\hat{v}_{c.rel}(\hat{x})}{\hat{v}_{drop}(\hat{x})}$			
10.3	$\frac{df_{DD}}{dP_c}$	$\int_0^1 K(\hat{x}) \cdot d\hat{x}$		$\frac{1}{2} \cdot \int_0^1 K(\hat{x}) \cdot \left(1+\cos\left(\omega \cdot \frac{T}{2} \cdot \hat{x}\right)\right) \cdot d\hat{x}$	$\int_0^1 K(\hat{x}) \cdot d\hat{x}$	$\frac{1}{2} \cdot \int_0^1 K(\hat{x}) \cdot \left(1+\cos\left(\omega \cdot \frac{T}{2} \cdot \hat{x}\right)\right) \cdot d\hat{x}$

tab. 2/1 Model Terms in Equation (1)

In lines 3.1 and 3.2 the terms Θ_{ox} and Θ_{fu} in equations (2) are given for the oxidizer and the fuel contribution. The differences for the LF and the HF oscillation cases result from the fact that (a) the intrinsic effects pulsing combustion and coolant film consumption are neglected (Klystron effect fully considered; see tab. 2/2, lines 3.1 and 3.2) for the LF case and (b) the steady- state nozzle equation (8) cannot be applied for the HF case.

The admittances $Y_{inj.ox.rel}$ and $Y_{inj.fu.rel}$ in equations (2) are determined in lines 8.1 and 8.2. They contain the propellant injection admittances related to the outlet areas of the injection elements. The propellant feed lines are described by series connections of elbows, bellows, pumps, turbines, throttles and straight tubes. The series connections are mathematically realized by a multiplication of the individual transfer matrices opposite to the flow direction. The injection elements are treated as the last tubes of the propellant feed lines.

$$\begin{pmatrix} \dot{m}' \\ P' \end{pmatrix}_{\mathrm{inj}} = \prod_{i=1}^{n} A_{n+1-i} \cdot \begin{pmatrix} \dot{m}' \\ P' \end{pmatrix}_{\mathrm{tank}} = B \cdot \begin{pmatrix} \dot{m}' \\ P' \end{pmatrix}_{\mathrm{tank}} \tag{5}$$

When applying the tank boundary condition, the injection admittance results (equation (6)). In case of complex feed lines, particularly for LF analyses, the matrix coefficients can also become quite complex. For HF cases, often the limitation to the injection elements suffices what simplifies the matrix coefficients to physics of one straight tube. This determination procedure is identically applied for the oxidizer and fuel lines.

$$Y_{inj} = -\frac{b_{12}}{b_{11}} \tag{6}$$

The admittance $Y_{ms.rel}$ in line 4 from equation (3) describes the capability of the combustion chamber to dynamically store mass. The technical measure of storage capability is the residence time Θ_c of the gas in the combustion chamber.

$$\Theta_c = \frac{m_c}{\dot{m}_c} = \frac{l^* \cdot c^* \cdot \eta_{c^*}}{a^2} \tag{7}$$

This admittance is directly proportional to the frequency, i.e. the higher frequency is the more damps the combustion chamber volume. This is the reason why combustion chambers with big volumes or small propellant mass flow rates are unlike to become unstable, provided the disturbances from the feed lines are not too severe (admittances $Y_{inj.ox.rel}$ and $Y_{inj.fu.rel}$).

The next two admittances $Y_{Pc.rel}$ and $Y_{vc.rel}$ in the lines 5 and 6 derive from the chamber flow equation. The following equations apply (equation (8) for the LF case and equation (9) for the HF case).

$$\dot{m}_c = \frac{A_{th} \cdot P_c}{c^* \cdot \eta_{c*}} \tag{8}$$

$$\dot{m}_c = A \cdot \rho_c \cdot v_c \tag{9}$$

Both equations are linearized and Laplace transformed. For equation (9), additionally, isentropic condition is supposed as well as the nozzle admittance definition α_{irr} of Bell/ Zinn [15] applied. The distributed gas velocity in the combustion chamber must be considered for $Y_{Pc.rel}$ in case of longitudinal modes what then provides an additional damping. It is noted that the pressure- related admittance $Y_{Pc.rel}$ is positive and, therefore, always stabilizing, whereas the velocity- related admittance $Y_{vc.rel}$ may also be negative depending on the value of α_{irr} as a function of nozzle geometry and mode shape.

The droplet drag admittance $Y_{DD.rel}$ in equation (3) is defined in line 7 and considers the energy loss from the interaction between the propellant droplets and the combustion gas. The corresponding terms are presented in lines 10.2 and 10.3. The assumption behind is that, at each axial position in the combustion chamber, a certain amount of liquid propellant mass is present. The injected propellant droplet sizes are determined from given experimental correlations and their consumption is determined from the relative velocity between combustion gas and droplet. To get the total droplet drag, the term given in line 10.2 is integrated along the combustion chamber axis. Since distributed velocities are considered and droplet drag is assumed to solely depend on pressure, longitudinal modes require the consideration of the mode shape leading to a reduction of damping. This is in contrast to line 1.3 where combustion gain reduction increases stability margin.

Finally, the admittance of the acoustic absorbers $Y_{abs.rel}$ is defined in line 9. The absorbers are treated like the feed lines for $Y_{inj.rel}$ in lines 8.1 and 8.2 (see equation (6)) but with the closed end condition instead of the tank condition. The total admittance is the single absorber admittance times the number of identical absorbers. This is repeated for each absorber class and, finally, delivers Y_{abs} of the total absorber ring.

It is noted that the model doesn't consider any spatial distribution of absorbers. This means that, particularly for tangential modes, the damping effect of the absorber ring is overestimated. This requires a correction by parameter η_{abs}. For radial and longitudinal modes this correction is not needed, because then the absorber ring operates uniformly at the right place near the closed end of the combustion chamber.

Parameter Settings

In the equations and model terms several parameters occur which must be known from experience, model adaptation to test data or literature. Otherwise, assumptions must be undertaken. In tab. 2/2 the essential model parameters are introduced.

Equation (1) constitutes the balance condition between instability drivers and instability dampers. This condition can be utilized to iteratively solve its real and imaginary parts for two unknown parameters at times when also measurement data indicate such a balance. For the future, it is foreseen to implement STABAN into an optimization algorithm to simultaneously fit all parameters to a sufficient number of tests.

In the lines 1.1 and 1.2 of tab. 2/2 the total combustion time lags of oxidizer $\tau_{t.ox}$ and fuel $\tau_{t.fu}$ are depicted (see equations (2)). They are determined by iterating equation (1) for the LF case. The other model parameters take on the values as given in tab. 2/2. These values derive from the agreement that intrinsic effects inside the combustion chamber play no role for the black box approach, except the Klystron effect known to be LF- related (see also tab. 2/1, lines 3.1 and 3.2). The total combustion time lags then are available for calculations in the HF range.

In a next step the model parameters A_c (see tab. 2/1, line 1.1) and $f_{Kly.ox}$/ $f_{Kly.fu}$ (see tab. 2/1, lines 3.1 and 3.2) are determined. The parameters $f_{Kly.ox}$ and $f_{Kly.fu}$ consider the fact that the LF- related Klystron effect would be overestimated in the HF range without correction. Typically, no difference is made for both the propellants. To find reasonable estimations for the absorber ring efficiency η_{abs} (see tab. 2/1, line 9), it is recommended to first take tests without absorbers (η_{abs}=0) or confine to radial or longitudinal modes for which absorber ring efficiency is maximum (η_{abs}=1). The parameter n_{32} (see tab. 2/1, lines 3.1 and 3.2) considers the impact of velocity variation on sensitive time lag τ_s (see tab. 2/1, line 1.1). This can normally be neglected compared to the pressure impact.

It is noted that this adaptation approach derives from practical experience. Depending on the specific case considered, any other combination of two parameters can be taken for iteration in the HF range. As an option, further adaptation calculations can follow for tangential modes to determine the parameter η_{abs} for this mode shape. The already known values of $\tau_{t.ox}$, $\tau_{t.fu}$ and $f_{Kly.ox}$=$f_{Kly.fu}$ are then utilized for the determination of the new A_c and η_{abs} for the tangential mode.

Finally, the last unknown parameter $G_{vc.rel}$ (see tab. 2/1, line 1.2) is determined in the HF range, if required and relevant for the thrust chamber operation. Equation (1) is again iterated at times when experimental data show a non- linear balance. A_c is determined as well assuming a modified combustion gain in this case.

Case		Linear Oscillations		Non- Linear Oscillations
Range		**LF**	**HF**	
1.1	$\tau_{t.ox}$	output	input	
1.2	$\tau_{t.fu}$	output	input	
2.1	A_c	0	output	output
2.2	n	0	0.5	
2.3	τ_s	0	input	
2.4	$G_{vc.rel}$	0		output
3.1	$f_{Kly.ox}$	1	output	input
3.2	$f_{Kly.ox}$	1	output	input
3.3	f_{fu}	0	input	
3.4	n_{32}	0		
4	d_{drop}	input		
5	η_{abs}	0	input	

tab. 2/2 Essential Model Parameters in Equation (1)

The sensitive time delay τ_s in line 2.3 is typically determined from the chamber resonance condition. The droplet sizes at injection (d_{drop} in line 4) are given by experimental correlations from literature or laboratory tests. The parameter f_{fu} in line 3.3 (see tab. 2/1, line 3.2) gives a constant ratio of coolant flow rate to total chamber flow rate in case of film cooled combustion chambers, otherwise it is zero. The interaction index n is 0.5 for coaxial injection elements [1]. In case all other parameters in tab. 2/2 are sufficiently known from previous adaptations for the same thrust chamber family, the effective injection droplet sizes d_{drop} can also be determined by equation (1) for the HF case.

3 Model Validation Approach

The basic approach of model parameter determination is already described in chapter 2. In the following two particularly interesting aspects are highlighted in more detail.

Total Combustion Time Lags

Additionally to the iterative approach described in chapter 2, a second method exists for the determination of the combustion time lags from the experimental pressure loss oscillations across the injection elements.

In the left part of fig. 3/1 a time interval is shown in which an oscillation of the relative injection pressure loss on the oxidizer side exists with constant amplitude. Consequently, resonance is given between oxidizer dome and combustion chamber. On fuel side, the oscillation amplitudes of the relative injection pressure drop are much smaller and not so clearly organized, because fuel is gaseous here.

The calculation results for the oxidizer are introduced on the right side of fig. 3/1 of which the interval, shown on the left side constitutes one single dot. A noticeable dispersion around τ_t=0.9ms is given indicating that resonance frequencies correspondingly change from interval to interval. It is noted that such resonance oscillations are typically taken from combustion noise, since specific test goals for subsequent systematic and well- defined stability analyses are rarely considered and stability aspects are mostly treated only as passenger test objectives.

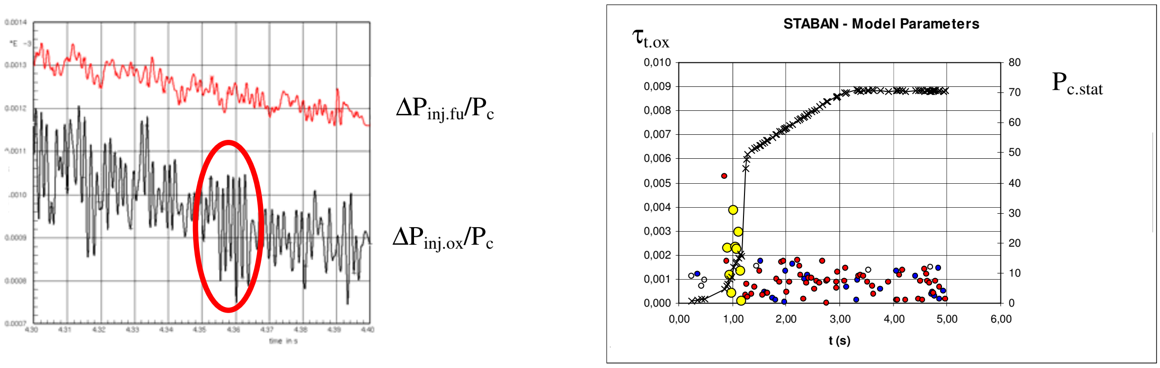

Fig. 3/1 Determination of the Total Combustion Time Lags from Pressure Phase Shifts

The figure below introduces the way described in chapter 2. In this case equation (1) is iterated for the LF case (see tab. 2/2, lines 1.1 and 1.2). The mean operation conditions are calculated for each interval where the combustion chamber pressure oscillation is zero. The calculation result is shown on the right side.

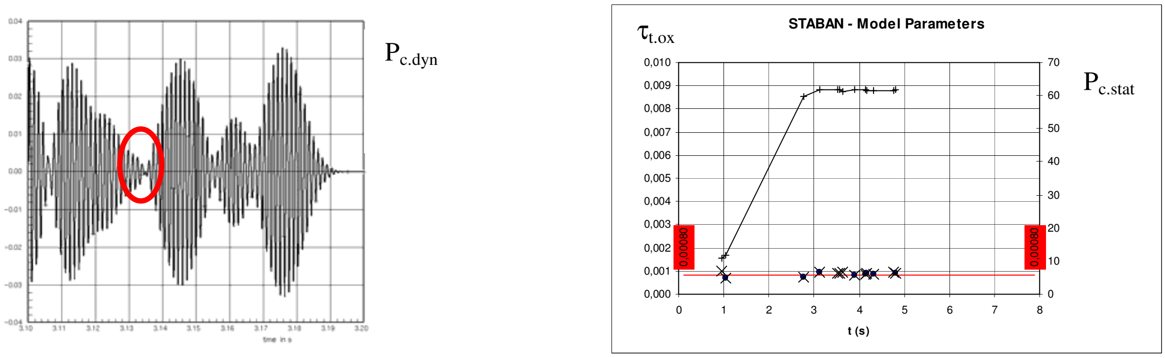

Fig. 3/2 Determination of the Total Combustion Time Lags from Forced Condition Iteration

The existence of two parallel calculation approaches facilitates the determination of the most probable values of these essential but hidden quantities. Here, the iteration approach confirms the mean value in fig. 3/1. As a further aspect, the mathematical parameter can be proven to be consistent with the physical quantity.

Absorber Parameters

Three parameters are to be considered for absorber model validation. They are the resistance factor Γ_{abs}, the effective fluid temperature T_{abs} inside the absorber and the absorber length correction Δl_{abs} for a theoretical absorber extension into the combustion chamber to account for flow coupling effects.

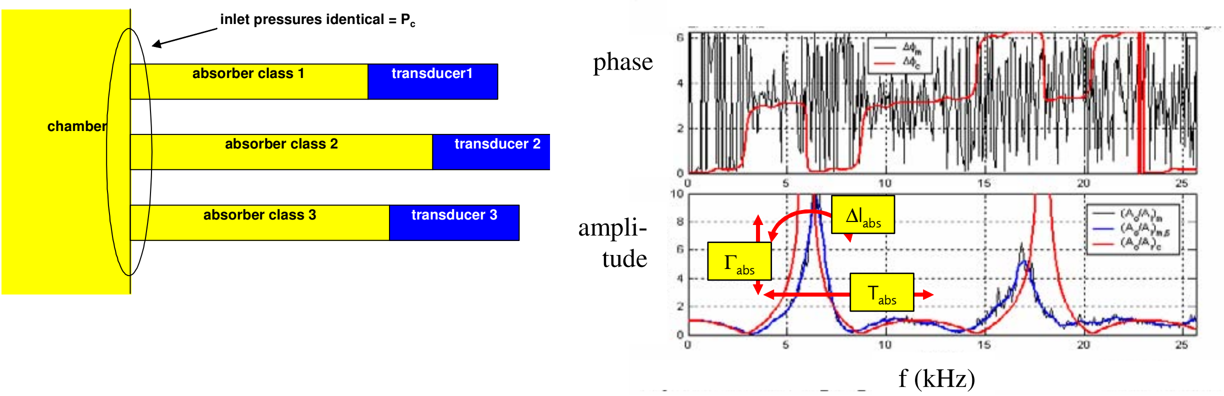

Fig. 3/3 Absorber Model Validation

The calculated (red) curves can be efficiently adjusted to the experimental (black) curves for amplitude and phase. The blue curve represents a filtered version of the black amplitude curve. The jumps between zero and 2π as well as the nervous behaviour of the experimental phase curve, deriving from sensor characteristics, are not relevant for the model adaptation. It is noted that a good agreement between STABAN results and test is obviously reached for frequencies below 10kHz. This is the interesting frequency bandwidth for the thrust chamber considered. Beyond this limit, internal absorber effects from linear viscous and thermal wall resistances [13] increasingly dominate, since they are proportional to the square root of frequency, making deviations between model and experiment greater.

$$R_{abs} = \frac{\Gamma_{abs} \cdot |\dot{m}'|}{\rho_{abs} \cdot A^2} \tag{10}$$

In STABAN equation (10), which describes the non- linear resistance from flow losses around the absorber's inlet edges, is utilized for model validation in which Γ_{abs} is the resistance factor for the flow losses around the absorber's inlet. With this value the red amplitude curve can be vertically shifted. The effective fluid temperature T_{abs} is indirectly considered by the fluid properties (like in equation (5) for the feed lines) and shifts the red amplitude curve horizontally. Normally, these parameters are sufficient for model validation purposes. In parallel, also the impact on the red phase curve must be monitored to get the best fit. The following figure refers to a thrust chamber with liquid propellants. A physical law could be found for Γ_{abs} for a specific absorber class in the absorber ring.

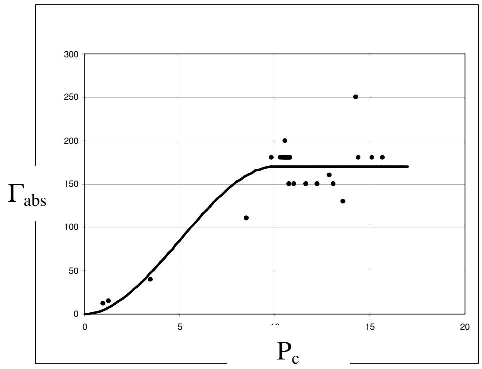

Fig. 3/4 Typical Physical Law for the Absorber Resistance Factor Γ_{abs}

4 Stability Calculations

The applicability range of STABAN confines to the hardware adjusted to. With less accuracy but still valid, it can also be applied inside a family of thrust chambers. Those families are characterized by identical propellant pairs and comparable designs of essential hardware parts. The following main engineering activities are typical for the layout of rocket propulsion systems:

- adjustment of the feed lines to operational requirements and geometrical stage constrains
- choice of the inner contour of the combustion chamber and the exhaust nozzle
- decision for the kind of propellants
- design of the injector, particularly of the injection elements
- definition of the operation control from valve opening until main stage operation

All of them determine the dynamic behavior of the system in a coupled manner. Still, the most important criteria for the classification into families are the propellants and the design of the injection elements. Their choice must be decided already in an early development phase. Any modification of propellants or injection elements moves the thrust chamber to another family necessitating a new process of model validation. In late development phases a severe risk then arises with respect to time schedule and costs.

The other engineering activities named above can be modified without a loss of simulation reliability and without risking family membership, as long as the modifications don't exceed the given validity ranges of the fluid property tables and the physical correlations applied. By changing the feed lines, the inner combustion chamber contour and the operation control, an optimum solution can be found for a given thrust chamber family for instability risk prevention. Sensitivity studies may accompany to get an imagination how susceptible the thrust chamber is to potential design changes. The dynamic good nature, found out by sensitivity studies, should be a criterion for the choice of future hardware concepts to avoid problems in case of later redesigns.

Chugging Analyses

For LF analyses the feed lines gain more importance at the expense of the combustion chamber which practically then serves just as a dynamic boundary condition (black box). The increased importance of the feed lines is reflected by a finer distribution of model tubes to consider local effects (see equation (5)).

Considering the terms in tab. 2/1 for the LF case, equation (1) takes the form given by equation (12) for chugging analyses. Equation (12) is taken from [2]. Here, the values of the constants a and b are both 0.5.

$$-1 = \frac{e^{-\sigma_m s}}{\theta_g s + 1}\left[e^{-\sigma_{v,o} s} \frac{a}{\frac{\overline{\Delta P}_{I,o}}{\overline{P}_C}} \left(\frac{\overline{R}}{\overline{R}+1} + \overline{R}\,\frac{\overline{\frac{\partial C^*}{\partial R}}}{C^*} \right) + e^{-\sigma_{v,f} s} \frac{b}{\frac{\overline{\Delta P}_{I,f}}{\overline{P}_C}} \left(\frac{1}{\overline{R}+1} - \overline{R}\,\frac{\overline{\frac{\partial C^*}{\partial R}}}{C^*} \right) \right] \tag{12}$$

With this equation, stability limit analyses can be performed for various total combustion time lags [2]. The relative injection pressure drops are taken as the axis values in fig. 4/1 (see also fig. 4/4, left side).

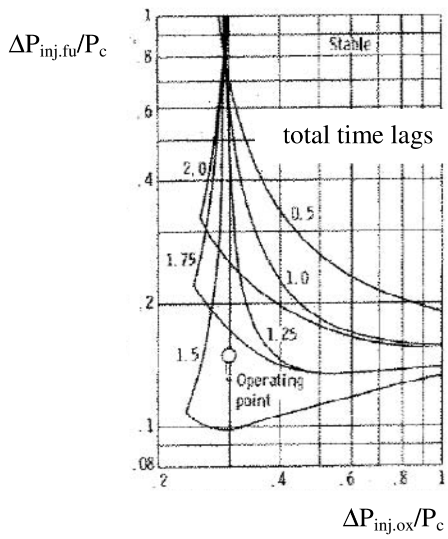

Fig. 4/1 Stability Limits for Different Total Combustion Time Lags

The lines of constant time lag in fig. 4/1 are the border lines between stability and instability. When walking clockwise along the lines, the area on the right hand side is the stable region. On the left side instability is given. From the calculations results the interesting fact that, when increasing the time lag, the stable region extends also to very small relative injection pressure drops what is opposite to the common opinion that instability risk rises with increasing time lag. Still, at a certain limit time lag (here: 1.5ms) the situation changes to the opposite and the unstable region again rises. Such limit time lags were first seen in experiments [2] and couldn't be explained from experience. The theory behind equation (1), which is identical to equation (12) for LF oscillations, confirms these experimental findings what, therefore, constitutes a practical plausibility check for STABAN for LF cases.

Stability Curves

Stability curves are time plots of the system eigenvalue for the HF case. The eigenvalue uniquely expresses whether a system is unstable (positive) or stable (negative).

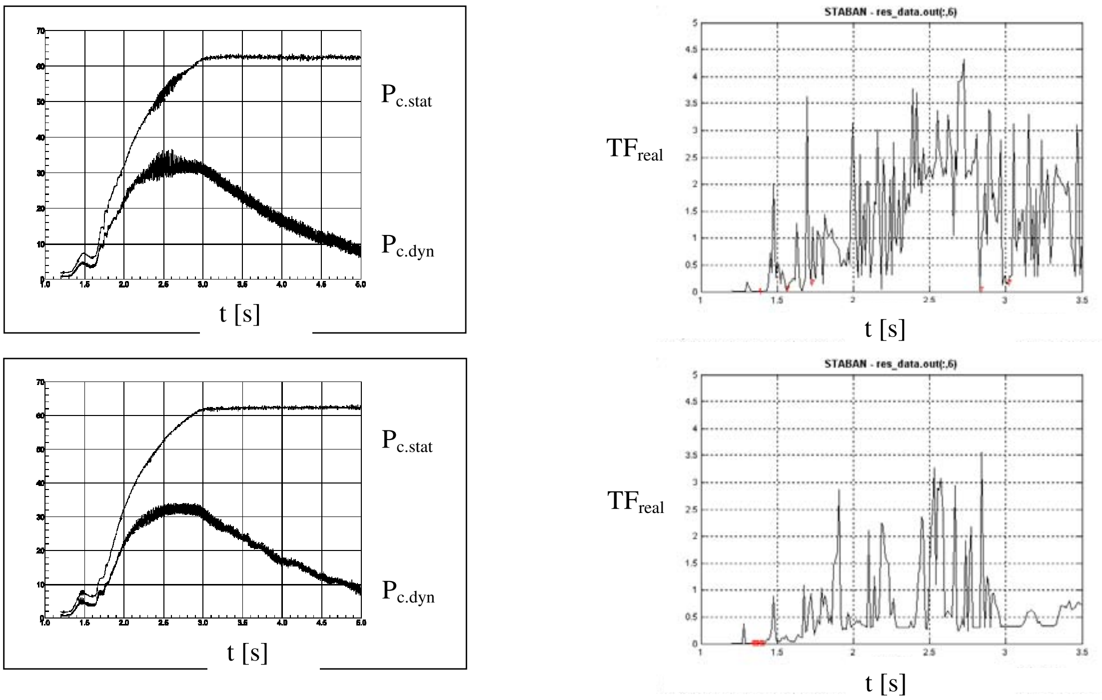

Fig. 4/2 Stability Curves for Different Dynamic Cases (real part of transfer function)

It is noted that for the above figure the real part of the transfer function is plotted. Here is instability above 1 and stability below 1. Two tests with a cryogenic thrust chamber, supposed to be identical, are presented. The pressure sensor data of the combustion chamber pressure (static and dynamic sensors) shows a short instability in the upper test but none in the lower one. STABAN was applied to detect hidden reasons for this difference. The calculation results on the right side show that STABAN detects similar situations. For the upper case the unstable range is confirmed (around t=2.5s). The stable case is also confirmed, since the real part remains below 1. The steep peaks need not be particularly considered, because they originate from local iteration problems or experimental data inaccuracies (see also fig. 3/3).

Another example is given in fig. 4/3 showing the behavior of another thrust chamber with liquid propellants. The stability curve (bottom) now shows the system eigenvalue indicating stability if negative or instability if positive. The experimental diagram (top) and the calculation result (bottom) are time- correlated to facilitate comparisons. The general statement on STABAN's plausibility from fig. 4/2 can be detailed in fig. 4/3. After a short peak, the measured dynamic pressure amplitude steadily increases. The starting instability is confirmed by the increase of the eigenvalue to positive values. After having reached a maximum value, the pressure amplitude again reduces to a minimum and finally reaches a limit cycle. In the eigenvalue plot, the situation is given fully comparably: The eigenvalue falls down to negative (stabilizing) and then reaches limit stability around zero. After the limit cycle the eigenvalue starts falling down what also makes pressure amplitude decreasing, and the situation becomes stable again.

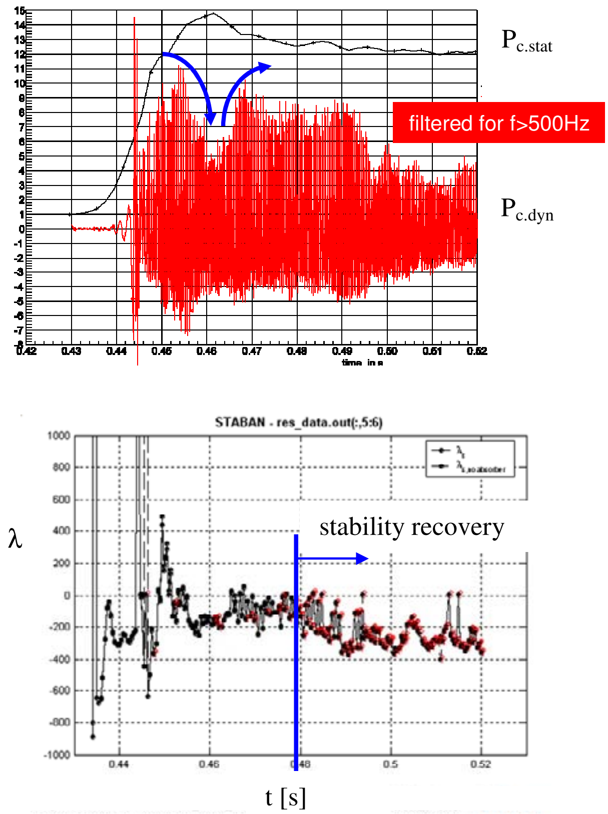

Fig. 4/3 Stability Curve (system eigenvalue)

Stability Mappings

The stability curves are particularly interesting for the detection and explanation of unexpected instability risks in acceptance or qualification tests to define quick countermeasures, be they hardware redesigns or operation control modifications from test to test. Since these calculations require test data like pressures and temperatures, they are not applicable in early development stages, except extrapolations from former development programs are feasible and fulfill the family requirements.

For parameter and sensitivity studies in early stages of development programs, the stability mappings are more suitable [9]. Two parameters are chosen which are considered essential for the elaboration of different design options and scattered around the expected main stage operation point or the probable startup range. STABAN calculates the stability risk in this field what finally gives a three- dimensional surface plot. The subsequent figure shows an example for a small scale thruster (left) with hypergolic propellants and a large scale thrust chamber (right) with green propellants. Both sides of the diagram refer to the T1 mode.

The left side of fig. 4/4 shows a safe startup (blue curve) up to main stage (yellow dot). The region critical to instability (red dots) is not touched or crossed. The safety margin can be directly determined as the numerical values of the relative injection pressure drops. They are major design criteria for injector layout. The oxidizer and the fuel are equally uncritical. The given plot is identical to fig. 4/1 with respect to the general shape of the stability limit line.

On the right side, the oxidizer mass flow (to the right) and the fuel mass flow (to the left) are chosen as the stability parameters. The ordinate gives the system eigenvalue. Isolated peaks originate from numerical iteration problems and can be neglected. The nominal main stage operation is indicated by the black line. The figure shows the sensitivity of the thrust chamber around this nominal condition. The flatter the area is the less nervous the thrust chamber reacts on operation variations due to physical dispersions or sudden and unexpected events from outside. This means that a prime development goal with respect to instability prevention should be to realize a flat eigenvalue surface below zero around the nominal operation point.

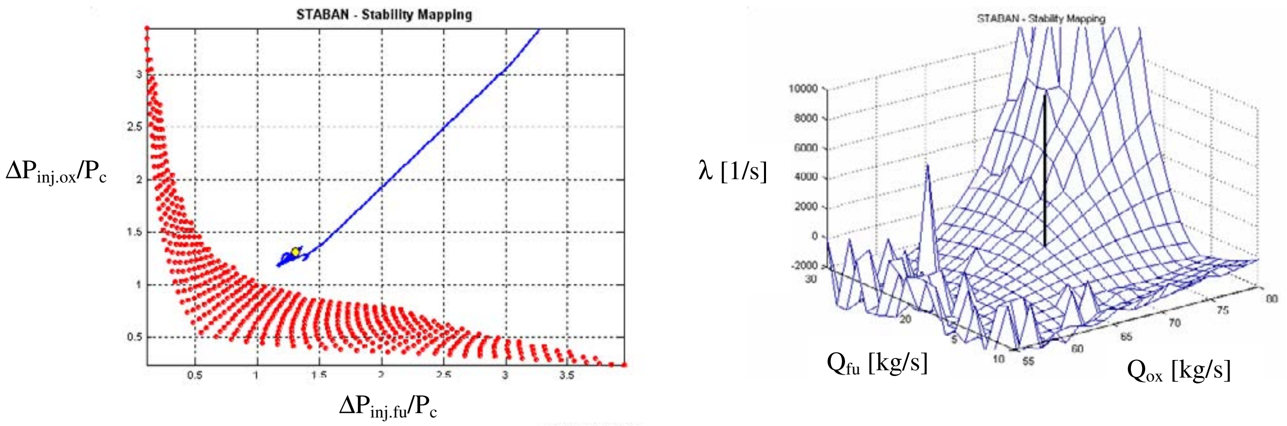

Fig. 4/4 Stability Mapping (left: rel. injection pressure drops, right: propellant flow rates)

Furthermore, it can be seen that, on the oxidizer side, an increase of mass flow rate continuously deteriorates the safety margin and increases the instability risk. On the fuel side, the situation is different. Going to higher mass flow rates at constant oxidizer flow rate, also increases instability risk, but less heavily, and it even seems that a maximum is reached. If the fuel mass flow rate is reduced from nominal, a minimum of the eigenvalue is reached indicating safe operation, but at further reduction the instability risk increases again. This means that, on fuel side, a clear optimum is given which can potentially be explained by the counteracting physical effects of feed line coupling, depending on injection pressure loss, and propellant jet preparation (total combustion time lag and droplet drag), depending on the injection velocity ratio. If the thrust chamber would be operated at this fuel flow optimum, nearly no dependency on oxidizer side would be given in a wide range of mass flow rate, i.e. the stability risk would be independent from the oxidizer side.

Safety Corridors

Another way of STABAN application is to determine safety corridors. They try to help defining proper startup corridors for the thrust chamber to minimize the risk for crossing critical regions or to optimize the hardware in these corridors that no instability problems can arise.

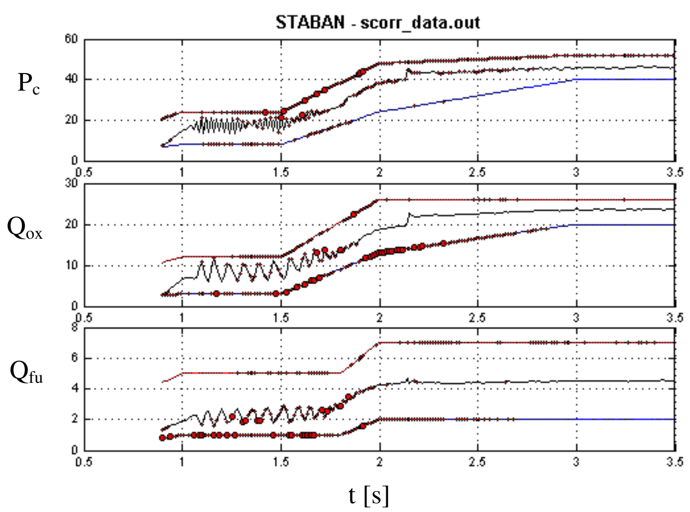

Fig. 4/5 Safety Corridors Around Thrust Chamber Startup Lines

The safety corridors given in fig. 4/5 refer to early investigations for a cryogenic thrust chamber and were applied to the combustion chamber pressure and the propellant mass flow rates as the main operation variables. The instability risk is calculated along these lines and in between for each variable and indicates potential instability risks by red points along the lines. Thereby, the size of the red points indicates how far the eigenvalue is above zero (see also fig. 4/4, right side), i.e. how significant the risk for instability is.

From a quick inspection of fig. 4/5 can be derived that chamber pressure is quite uncritical in the chosen corridor in this specific case, whereas the oxidizer and fuel mass flow rates are still critical at the low corridor boundaries, and that for oxidizer more at late startup and for fuel more at early startup. The mass flow corridors may be further investigated and newly defined or the hardware partly redesigned to improve the situation.

6 Summary and Conclusions

STABAN has acquired a solid state of modeling but requires further effort to consolidate and extend the approaches. By a systematical application of STABAN a new industrial standard can be established for future development programs in the field of instability prevention benefiting from the continuously increasing knowledge in the French- German REST group and the permanently improved model validation level. STABAN can be utilized to define thrust chamber test campaigns, to qualify the hardware against stability specifications and to provide a stability data base from systematic thrust chamber test analyses. Some application examples show promising perspectives for a general use of STABAN in future thrust chamber development programs in order to reduce the development risk with respect to instability.

The semi- empirical kind of STABAN limits its application to certain boundary conditions. Predictions are most reliable for thrust chambers of the same family. Families are classified by two prime engineering decisions: the choice of propellants (fluid properties), and the injection element design (dynamic feed line coupling and jet preparation). The propellants and the injection system should be solidly defined already in an early development phase and then kept unchanged not to make later predictions or extrapolations for instability risk estimation invalid or to necessitate additional model validation efforts.

The present paper just introduces the main models of STABAN to keep the volume at reasonable limits. There is a considerable number of accompanying models which are not mentioned or described. Beside others, they account for secondary coupling effects, distributed quantities in the combustion chamber, linear and non- linear resistance modeling, effective sonic velocity treatment and the consideration of measurement adapters, be they purged or not. A further considerable numerical effort is required for measurement data management and correction.

Acknowledgement

The activities for the STABAN development and also Astrium's participation in the French- German REST group are parts of the German TEKAN project which is substantially co- funded by the DLR.

The REST group has essentially contributed to STABAN by the frank and valuable scientific and technical discussions in the past decade and the research results helped to complete it for industrial use. In the REST group, the cooperation with the DLR, Lampoldshausen, is particularly highlighted for their readiness for test data exchange and interest in the modeling progress. Geoff Searby from the IRPHE, Marseilles, has also contributed to the overall understanding and supported the engineering viewpoint of the problem. Particularly, I thank Paul Spagna for his patient explanations and the practical case studies from decades of experience.

References

[1] D. T. Harrje, F. H. Reardon, *Liquid Propellant Rocket Combustion Instability*, NASA SP-194, 1972

[2] L. M. Wenzel, J. R. Szuch, *Analysis of Chugging in Liquid- Bipropellant Rocket Engines Using Propellants With Different Vaporization Rates*, NASA TN D-3080, 1965

[3] R. S. Valentine, *Liquid Rocket Performance, Stability, and Compatibility*, J. Spacecraft, Vol. 9, No. 5, 1972

[4] J. E. Pieringer, *Simulation selbsterregter Verbrennungsschwingungen in Raketenschubkammern im Zeitbereich*, Thesis, Technische Unversität München, 2008

[5] R. Lecourt, R. Foucaud, *Acoustic Sensitivity Measurements of Injectors in a Small Liquid Propellant Rocket Engine*, AIAA book, chapter 15, 1995

[6] J. E. Portillo, J. C. Sisco, M. J. Corless, V. Sankaran, W. E. Anderson, *Generalized Combustion Instability Model*, AIAA 2006-4889, 2006

[7] F. Richecoeur, P. Scouflaire, S. Ducruix, S. Candel, *Interactions between propellant jets and acoustic modes in liquid rocket engines: experiments and simulations*, AIAA 2006-4397, 2006

[8] J. C. Oefelein, V. Yang, *Comprehensive Review of Liquid- Propellant Combustion Instabilities in F-1 Engines*, J. Propulsion and Power, Vol. 9, No. 5, 1993

[9] R. C. Cavitt, R. A. Frederick, *Laboratory Scale Survey of Pentad Injector Stability Characteristics*, J. Propulsion and Power, Vol. 24, No. 3, 2008

[10] C. H. Sohn, A. A. Shibanow, V. P. Pikalov, *Combustion Stability Boundaries of the Subscale Rocket Chamber with Impinging Jet Injectors*, J. Propulsion and Power, Vol. 23, No. 1, 2007

[11] Y. C. Yu, L. A. O'Hara, J. C. Sisco, W. E. Anderson, *Experimental Study of High- Frequency Combustion Instability in a Continuously Variable Resonance Combustor (CVRC)*, AIAA 2009-234, 2009

[12] G. Searby, *Investigations of the dynamics of injectors coupled via the feed dome*, CNES-BC 4700024370, Intermediate Progress Report, 2009

[13] G. Searby, A. Nicole, M. Habiballah, E. Laroche, *Prediction of the Efficiency of Acoustic Damping Cavities*, J. Propulsion and Power, Vol. 24, No. 3, 2008

[14] P. Spagna, K. Vollmer, J. Keppeler, E. Boronine, *An Engineering View on LF- and HF Oscillation Inside Combustion Chambers,* 4th International Conference on Launcher Technology, Liège, 2002

[15] W. A. Bell, B. T. Zinn, *The Prediction of Three- dimensional Liquid- Propellant Rocket Nozzle Admittances*, NASA CR-121129, 1973